FORM TI-12
07/1999

B-T-3396

Application of a Sixth Order Generalized Stress Function To Determine Limit Loads for Plates with Triangular Penetration Patterns

J. L. Gordon
D. P. Jones

DE-AC11-98PN38206

BETTIS ATOMIC POWER LABORATORY WEST MIFFLIN, PENNSYLVANIA 15122-0079

Operated for the U.S. Department of Energy
by Bechtel Bettis, Inc.

Application of a Sixth Order Generalized Stress Function for Determining Limit Loads for Plates with Triangular Penetration Patterns

J. L. Gordon* and D. P. Jones*
Bechtel Bettis, Inc
West Mifflin, PA 15122-0079

*Member, ASME

ABSTRACT

The capability to obtain limit load solutions of plates with triangular penetration patterns using fourth order functions to represent the collapse surface has been presented in previous papers. These papers describe how equivalent solid plate elastic-perfectly plastic finite element capabilities are generated and demonstrate how such capabilities can be used to great advantage in the analysis of tubesheets in large heat exchanger applications. However, these papers have pointed out that although the fourth order functions can produce sufficient accuracy for many practical applications, there are situations where improvements in the accuracy of in-plane and transverse shear are desirable. This paper investigates the use of a sixth order function to represent the collapse surface for improved accuracy of the in-plane response. Explicit elastic-perfectly plastic finite element solutions are obtained for unit cells representing an infinite array of circular penetrations arranged in an equilateral triangular array. These cells are used to create a numerical representation of the complete collapse surfaces for a number of ligament efficiencies (h/P where h is the minimum ligament width and P is the distance between hole centers). Each collapse surface is then fit to a sixth order function that satisfies the periodicity of the hole pattern. Sixth-order collapse functions were developed for h/P values between .05 and .50. Accuracy of the sixth order and the fourth order functions are compared. It was found that the sixth order function is indeed more accurate, reducing the error from 12.2% for the fourth order function to less than 3% for the sixth order function.

NOMENCLATURE

P	Distance between penetration centers, mm
h	Minimum ligament width, mm
μ =	*h/P* Ligament efficiency
σ_i	Stress components for i = xx,yy,zz,xy, MPa
$S_0 = \mu S_y$	Effective yield stress of EQS material, MPa
S_y	Yield stress, MPa
$B_1,\ldots,B_4$	Coefficients for fourth-order collapse function
$C_1,\ldots C_7$	Coefficients for sixth-order collapse function
Y, Z_1,Z_2,Z_3	Out-of-plane constants for collapse function
E, ν	Young's modulus and Poisson's ratio of base metal
E*/E, ν*	Equivalent solid effective elastic constants
EQS	Equivalent solid
EPP	Elastic perfectly plastic
s_1,s_2,s_3	Transformed EQS stress components, MPa

INTRODUCTION

References [1, 2, 3, and 4] develop the use of a fourth-order function

$$\sigma_{eff} = \{\frac{1}{4}[B_1(\sigma_{xx}+\sigma_{yy})^4 + B_2[(\sigma_{xx}-\sigma_{yy})^2+4\tau_{xy}^2]^2$$

$$+ B_3(\sigma_{xx}+\sigma_{yy})^2[(\sigma_{xx}-\sigma_{yy})^2+4\tau_{xy}^2]$$

$$+ B_4(\sigma_{xx}^2-\sigma_{yy}^2)[(\sigma_{xx}-\sigma_{yy})^2-12\tau_{xy}^2]]^{0.5}$$

$$+ Y[\sigma_{zz}^2 - Z_3\sigma_{zz}(\sigma_{xx}+\sigma_{yy})] + 3Z_1\tau_{yz}^2 + 3Z_2\tau_{zx}^2\}^{0.5}$$

$$= S_o \qquad (1)$$

to describe the plastic collapse of a perforated plate with a triangular penetration pattern. This collapse function was used by Jones and Gordon [4] to develop an elastic-perfectly plastic equivalent solid plate [EPP-EQS] flow theory that is useful in computing limit loads of perforated plates using conventional finite element analyses [FEA] programs. Utilizing comparisons with three dimensional FEA explicitly modeled perforated plates, the EPP-EQS solutions based on the fourth order solutions have been shown [5] to be reasonably accurate for plates with moderate ligament efficiencies (0.15<=h/P<=0.5) subjected to equal biaxial loads. For h/P < 0.15 and/or for situations with in-plane and out-of-plane shear loads, the accuracy may be less than desired.

Reinhardt [6] has suggested that improved accuracy may be possible using a sixth order function of the stress components. Since the out-of-plane (z-direction) response is treated in the same quadratic fashion in both the fourth and sixth order functions, it is not considered in this paper although it was included in the development.

Using the transformation

$$\begin{Bmatrix} s_1 \\ s_2 \\ s_3 \end{Bmatrix} = \begin{Bmatrix} (\sigma_{xx} + \sigma_{yy})/2 \\ (\sigma_{xx} - \sigma_{yy})/2 \\ \tau_{xy} \end{Bmatrix} \tag{2}$$

to simplify the formulation allows the collapse surface in the plane of the penetrations to be written as

$$\begin{aligned} \sigma_{eff} = \{ & [C_1 s_1^6 + C_2 s_1^4 (s_2^2 + s_3^2) + C_3 s_1^2 (s_2^2 + s_3^2)^2 \\ & + C_4 (s_2^2 + s_3^2)^3 + C_5 s_1^3 s_2 (s_2^2 - 3 s_3^2) \\ & + C_6 s_1 s_2 (s_2^2 + s_3^2)(s_2^2 - 3 s_3^2) \\ & + C_7 \{ s_2^2 (s_2^2 - 3 s_3^2)^2 - s_3^2 (s_3^2 - 3 s_2^2)^2 \}]^{1/3} \\ & + Y[\sigma_{zz}^2 - Z_3 \sigma_{zz} (\sigma_{xx} + \sigma_{yy})] + 3 Z_1 \tau_{yz}^2 + 3 Z_2 \tau_{zx}^2 \}^{0.5} \end{aligned} \tag{3}$$

Reinhardt has demonstrated that Eq. (3) displays the needed hexagonal symmetry necessary for a triangular pattern. The purpose of this paper is to evaluate the sixth-order function to see if improvements are possible relative to the fourth-order function and to evaluate its use in developing an EPP-EQS flow theory for calculating limit loads of perforated plates using FEA.

GEOMETRY AND LOADING CONDITIONS

Consider an infinite array of penetrations arranged in an equilateral pattern as shown in Figure 1. If the penetrations are very small compared to all other dimensions of the structure, symmetry of the deformation of an infinite array of such penetrations allows the identification of a unit cell that can be used to analyze the response of the pattern to general far field loading. The unit cell is shown in Figure 2.

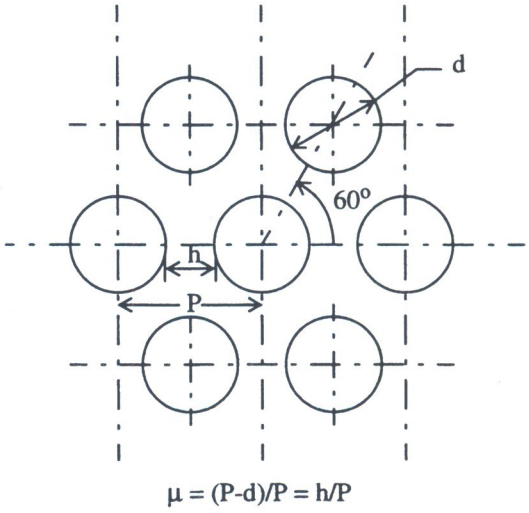

Figure 1. Penetration pattern.

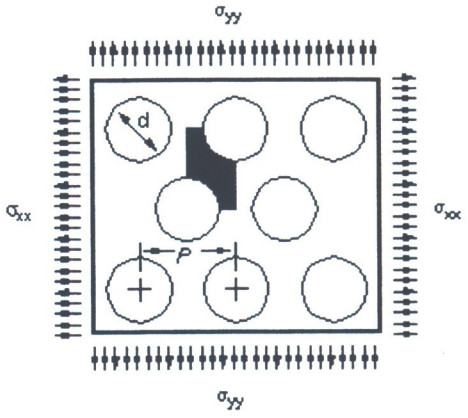

Figure 2. Unit Cell.

Limit load solutions are sought for the unit cell for various ratios of loading along the x and y axes. By determining the loads for which any additional increment of load causes plastic collapse of the unit cell, a collapse surface is obtained which is appropriate for assessing the

load interaction effects on the limit load of a perforated plate.

A basic two-dimensional (2D) generalized plane strain EPP-FEA model is used to obtain the collapse surfaces. The pitch was held constant and the radius of the penetration was varied to obtain the various *h/P* models. Ligament efficiencies of 0.05, 0.10, 0.15, 0.20, 0.30, and 0.50 were investigated. Young's modulus and Poisson's ratio were chosen to be 26.0E+6 psi (200E+3 Mpa) and 0.3, respectively. The yield strength was taken to be S_y = 0.002E. Since linear geometry assumptions are used, the limit loads are proportional to yield strength and the actual value chosen is not important.

FEA MODELS

ABAQUS [7] was used to obtain the 2D-FEA solutions. An elastic-perfectly plastic stress-strain curve was used. The collapse load is defined in these analyses as the load for which a small increase in load produces a very large increase in deflection, i.e., the load-deflection curve approaches a slope of zero. Using linear geometry (small-strain, small deformation formulations), this load complies with the theoretical definition of a lower bound limit load.

The FEA mesh is shown in Figure 3. There are a total of 576 eight-node reduced integration generalized plane strain elements and 1857 nodes in each of the models.

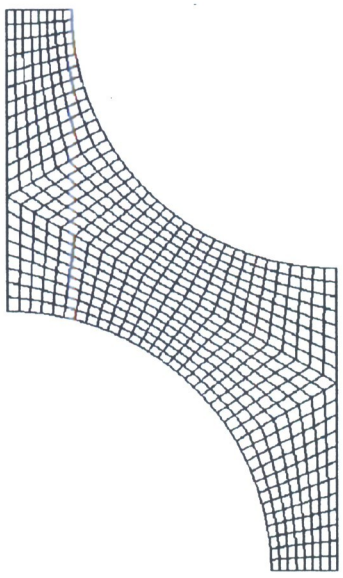

Figure 3. Explicit FEA Model.

The boundary conditions for the normal loads or ($\sigma_{x\,x}$, $\sigma_{y\,y}$) cases are shown in Figure 4. Surfaces A-B and E-F have symmetry boundary conditions – i.e. the displacements normal to these surfaces are zero and the forces tangential to them are zero. Surface D-E has the displacement components in the x direction constrained so that they are all equal – i.e. the face can only translate uniformly in the x direction. Similarly, surface B-C is constrained such that it can only translate uniformly in the y direction. The model is loaded by specifying the total forces, F_x and F_y, on faces D-E and B-C respectively. The loads F_x and F_y are specified independently. The equivalent solid stresses acting on the unit cell are

$$\sigma_{xx} = 2F_x/(\sqrt{3}P)$$

$$\sigma_{yy} = 2F_y/P \qquad (4)$$

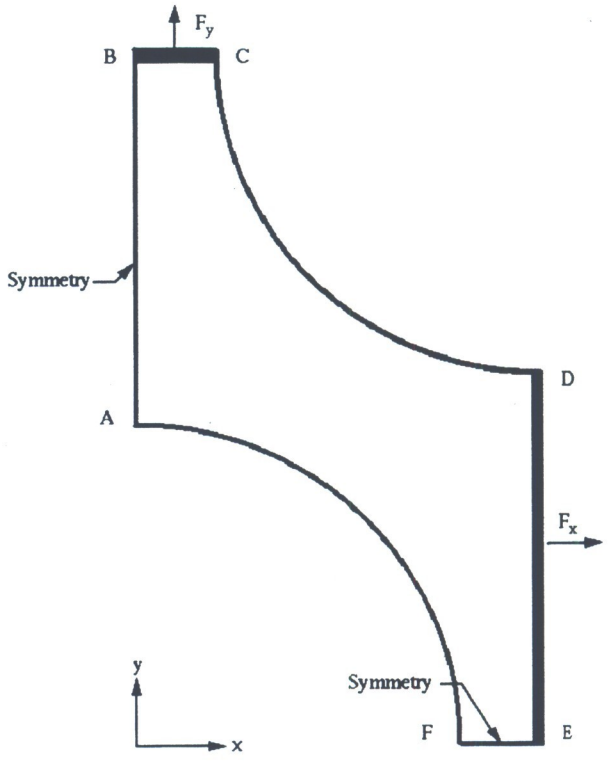

Figure 4. Boundary Conditions for F_x and F_y Case.

By varying F_x and F_y, a sufficient number of load cases are obtained to develop a full range of load ratios in quadrants one and four of the collapse surface. Results in quadrants two and three are obtained by reflection.

The boundary conditions for the shear case are shown in Figure 5. The surfaces B-C and E-F were constrained to displace δ_x uniformly in the tangential direction while

surfaces D-E and A-B displace δ_y uniformly in the tangential direction.

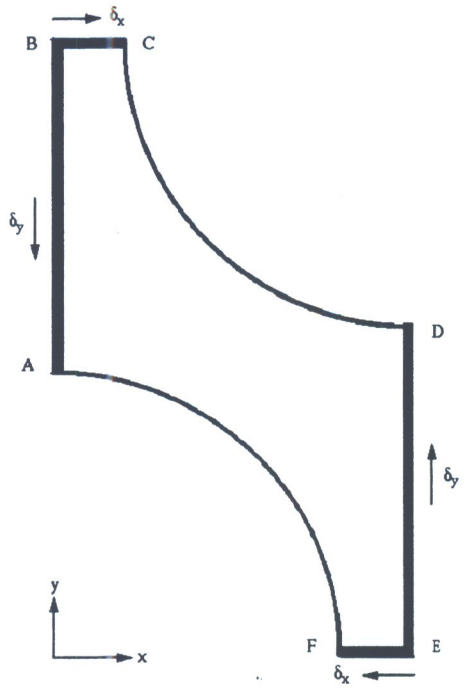

Figure 5. Boundary Conditions for F_{xy} Case.

Tangential displacements were defined on surfaces A-B and E-F while tangential forces were defined on surfaces B-C and D-E. This case allows for the direct solution of $(C_4 - C_7)$ from the equation

$$C_4 - C_7 = [\mu S_y / s_3]^6 \tag{5}$$

where s_3 is the equivalent solid shear stress that causes the unit cell to collapse due to the shear loading (Figure 5). If F_{xy} is the tangential load on surface D-E that causes the unit cell to collapse, then s_3 in Eq. (5) is

$$s_3 = 2F_{xy} / (\sqrt{3}P) \tag{6}$$

Similarly, surface B-C is constrained such that it can only translate uniformly in the y direction while keeping surface D-E straight with $F_x = 0.0$. The equivalent solid stresses acting on the unit cell are

$$\sigma_{xx} = 0.0$$
$$\sigma_{yy} = 2F_y / P \tag{7}$$

If F_y is the load on surface D-E that causes the unit cell to collapse, then using Equation (4), s_2 is

$$s_2 = 2F_y / (\sqrt{3}P) \tag{8}$$

This case allows for the direct evaluation of $(C_4 + C_7)$ by the equation

$$C_4 + C_7 = [\mu S_y / s_2]^6 \tag{9}$$

Eqs. (5 and 9) allow for the unique solution of C_4 and C_7.

MODEL VERIFICATION

Each of the FEA models was checked by first obtaining elastic solutions and comparing the equivalent solid plate effective constants for the various ligament efficiencies against other published results. Table 1 compares E*/E and υ* as a function of *h/P* with the values given in Slot [8]. Additionally, the peak elastic stress on the penetration surface is compared with Slot's [8] values to assure mesh adequacy. These values are also given in Table 1. Since the analysis results are all within 1% of the published values, it was judged that the mesh was adequate and the boundary conditions were applied properly for these models.

RESULTS

Figures 6, 7, and 8 show the collapse surfaces generated by the FEA results for $\mu = 0.05$, 0.2, and 0.50 which are representative of the ligament efficiencies used in the study. Tables 2 through 7 provide the data for all of the collapse surfaces. The MATHEMATICA [9] program was used to fit Equation (3) to the collapse surface data, Tables 2 through 7, by first calculating the $(C_4 + C_7)$ and $(C_4 - C_7)$ terms using Eqs. (5 and 9) to match the S_3 and S_2 cases given in Table 8 for each ligament efficiency. Then C_4 and C_7 can be determined. Coefficients C_1, C_2, C_3, C_5, and C_6 were then fit to the data points shown in the figures. All of the coefficients are given in Table 9.

The goal of this work is to investigate if improved accuracy is achieved with the sixth-order function over a wider range of ligament efficients than is possible with the fourth-order function. An error was calculated as a percentage for each explicit FEA point of the curve fit using the equation

$$e = [l - l_{FEA}]/l_{FEA} \tag{10}$$

In this equation, l_{FEA} is the length of a line from the origin to the FEA point while l is the length from the origin to the intersection point of l_{FEA} with the collapse surface. Both l and l_{FEA} are co-linear. The maximum and the average error for all FEA points are compared for each ligament efficiency and are provided in Table 10.

OBSERVATIONS

- The sixth order function error is less than 3% for $0.05 \le h/P \le 0.50$.
- The sixth order function reduces the error from 12.2% for the fourth order function to 2.3% for a ligament efficiency of 0.05.
- Figures 6, 7, and 8 show that the curvature of the sixth-order function is such that the normal to the surface is directed outward and the slope is not multi-valued at any point. Thus, the surface is always convex. This allows a flow theory to be developed based on the usual assumptions that strain increments are normal to the collapse surface. This is an important property for development of a flow theory since most commercial FEA plasticity programs are based on this assumption.

CONCLUSIONS

A sixth-order collapse surface is developed for thick perforated plates containing a triangular penetration pattern with ligament efficiencies of 0.05, 0.10, 0.15, 0.2, 0.3, and 0.5 using elastic-perfectly plastic FEA analysis. The FEA data was fit to a sixth-order collapse function and the resulting curves were compared to previously generated fourth-order collapse surfaces. Based on this work, the following conclusions are drawn:

- The sixth-order function improves accuracy over the fourth order function over the entire range of ligament efficiencies studied ($0.05 \le h/P \le 0.5$).
- Accuracy is improved from 12.2% for the fourth order function to less that 3% for the sixth order function.
- The sixth order function is suitable for development of an EPP-EQS flow theory because the surface is convex.

ACKNOWLEDGEMENT

The analysis presented here was performed under a U.S. Department of Energy contract with Bechtel Bettis, Inc. The authors are grateful to Ms. Virginia Ogurchak and Ms. Bernadette Holly for their help in preparing this document.

REFERENCES

[1] W. D. Reinhardt, 1998, "Yield Criteria for the Elastic Plastic Design of Tubesheets with Triangular Penetration Patterns", PVP Vol. 370, *Finite Element Applications: Linear, Non-Linear, Optimization and Fatigue and Fracture*, pgs. 113-120.

[2] Reinhardt, W., 1999, "A Fourth-Order Equivalent Solid Model for Tubesheet Plasticity," ," presented at the 1999 ASME PVP Conference, PVP-Vol. 385, *Computer Technology – 1999*, pgs 151-158.

[3] J. L. Gordon, Jones, D. P., Banas D., and Hutula, D. N., 1999, "A Collapse Surface for a Perforated Plate with an Equilateral Triangular Array of penetrations," presented at the 1999 ASME PVP Conference, PVP-Vol. 385, *Computer Technology – 1999*, pgs 125-134.

[4] D. P. Jones, J. L. Gordon, Hutula, D. N., Banas, D., Newman, J. B., 2001, "An Elastic-Perfectly Plastic Flow Model for Finite Element Analysis of Perforated Materials," ASME Journal of Pressure Vessel Technology, 123 No. 3, pgs. 265-270.

[5] D. P. Jones and J. L. Gordon, 2001, "Collapse Surfaces for Perforated Plates with Triangular Penetration Patterns for Ligament Efficiencies between 0.05 and 0.50," PVP-Vol. 47, Emerging Technologies: Advanced Topics in Computational Mechanics and Risk Management ASME 2001, pgs. 67-78.

[6] W. Reinhardt, 2000, "An Equivalent Solid Based Analysis of Broached Tube Support Plates," PVP-Vol. 400, *Emerging Technologies: Risk Assessment Computational Mechanics, and Advanced Engineering Topics ASME 2000*, pgs. 243-261.

[7] *ABAQUS: Theory Manual* Version 5.8, 1998, Hibbitt, Karlsson & Sorensen, Inc., Farmington Hills, MI.

[8] Slot, T., 1972, "Stress Analysis of Thick Perforated Plates," Ph.D. Thesis, Dept. of Mech. Engr., The University of Technology Delft, the Netherlands, Technomic Publishing Co., Inc.

[9] *MATHEMATICA 4.0 for Silicon Graphics*, 1999, A System for Doing Mathematics by Computer, Wolfram Research, Inc. Champaign, IL, USA.

Table 1. Elastic model verification.

h/P	*E*/E*	*ν**	σ_ϕ/σ_y @ *30°*
0.05 FEA	0.0172	0.8078	17.44
0.05 Slot	0.0172	0.8078	17.53
0.10 FEA	0.0521	0.6606	11.92
0.10 Slot	0.0520	0.6606	11.92
0.15 FEA	0.0994	0.5444	8.782
0.15 Slot	0.0994	0.5445	8.790
0.20 FEA	0.1553	0.4574	6.834
0.20 Slot	0.1553	0.4575	6.844
0.30 FEA	0.2805	0.3541	4.639
0.30 Slot	0.2806	0.3540	4.654
0.50 FEA	0.5447	0.2992	2.790
0.50 Slot	0.5446	0.2994	2.841

Table 2. Collapse data for $h/P = 0.05$.

Case	$\sigma_{xx}/\mu S_y$	$\sigma_{yy}/\mu S_y$
1	0.679053	1.176154
2	0	0.681231
3	0.626647	0
4	0.251503	-0.43562
5	0.25963	0.899231
6	0.157084	0.816154
7	1.183568	1.024615
8	0.720355	0.124769
9	0.835826	0.289538
10	0.972169	0.505077
11	1.107624	0.767308
12	1.162695	1.208462
13	0.99704	1.208462
14	0.872243	1.208462
15	0.775426	1.208462
16	1.197336	1.089231
17	1.209327	1.151538
18	1.21288	1.208462
19	0	-0.681231
20	0.154241	-0.534309
21	0.110851	-0.576077
22	0.489859	-0.169692
23	0.398505	-0.276077
24	0.334241	-0.347385
25	0.287121	-0.397846

*Full collapse surface obtained by symmetry.

Table 3. Collapse data for $h/P = 0.10$.

Case	$\sigma_{xx}/\mu S_y$	$\sigma_{yy}/\mu S_y$
1	0	0.931154
2	0.810955	0
3	0.709031	1.228077
4	0.345966	-0.61077
5	1.199112	1.038462
6	0.340193	1.178846
7	0.210733	1.095
8	1.001037	0.346923
9	1.142487	0.791538
10	1.181792	1.228077
11	0.886233	1.228077
12	0.212754	-0.73692
13	0.39437	-0.546538
14	0.152976	-0.795
15	0.655515	-0.22704
16	0.540933	-0.37481
17	0.457217	-0.47538
18	0	-0.931134

*Full collapse surface obtained by symmetry.

Table 4. Collapse data for $h/P = 0.15$.

Case	$\sigma_{xx}/\mu S_y$	$\sigma_{yy}/\mu S_y$
1	0	1.061538
2	0.881273	0
3	0.725833	1.257179
4	0.397187	-0.68795
5	1.225907	1.061795
6	0.362842	1.256923
7	0.235233	1.222308
8	1.032865	0.357692
9	1.16758	0.808974
10	1.209623	1.257179
11	0.90718	1.257179
12	0.244412	-0.84692
13	0.175574	-0.91256
14	0.731754	-0.25351
15	0.61288	-0.42462
16	0.521688	-0.54205
17	0.451666	-0.6259
18	1.252554	1.193333
19	0	-1.061538

*Full collapse surface obtained by symmetry.

Table 5. Collapse data for $h/P = 0.20$.

Case	$\sigma_{xx}/\mu S_y$	$\sigma_{yy}/\mu S_y$
1	0	1.188077
2	0.940267	0
3	0.786529	1.362308
4	0.447817	-0.77564
5	1.259956	1.091154
6	0	-1.18808
7	0.394967	1.368333
8	0.257217	1.336538
9	0.629534	-0.54526
10	1.094301	0.379103
11	1.254627	0.869231
12	1.166396	1.212179
13	0.955589	1.324103
14	0.27624	-0.95705
15	0.19815	-1.02949
16	0.800296	-0.27718
17	0.680459	-0.47141
18	0.584234	-0.60718
19	0.508142	-0.7041

*Full collapse surface obtained by symmetry.

Table 6. Collapse data for $h/P = 0.30$.

Case	$\sigma_{xx}/\mu S_y$	$\sigma_{yy}/\mu S_y$
1	0	1.188077
2	0.940267	0
3	0.786529	1.362308
4	0.447817	-0.77564
5	1.259956	1.091154
6	0	-1.18808
7	0.394967	1.368333
8	0.257217	1.336538
9	0.629534	-0.54526
10	1.094301	0.379103
11	1.254627	0.869231
12	1.166396	1.212179
13	0.955589	1.324103
14	0.27624	-0.95705
15	0.19815	-1.02949
16	0.800296	-0.27718
17	0.680459	-0.47141
18	0.584234	-0.60718
19	0.508142	-0.7041

Table 7. Collapse data for $h/P = 0.50$.

Case	$\sigma_{xx}/\mu S_y$	$\sigma_{yy}/\mu S_y$
1	0.787728	1.364385
2	1.313783	0.910231
3	0.468808	-0.812
4	0	1.243615
5	1.003479	0
6	0.260607	1.354154
7	0.398238	1.379538
8	0.65929	-0.57092
9	1.098253	0.190231
10	1.203331	0.416846
11	1.314049	0.682769
12	1.245122	1.078308
13	1.147772	1.192769
14	1.045004	1.267
15	0.948942	1.314923
16	0.863005	1.345308
17	0.289297	-1.00215
18	0.20758	-1.07854
19	0.841999	-0.29169
20	0.713028	-0.494
21	0.611769	-0.63577
22	0.532184	-0.73746
23	0	-1.243615

*Full collapse surface obtained by symmetry.

Table 8. Collapse data for shear case.

h/P	$C_4 - C_7$	$C_4 + C_7$
0.05	1403.84	645.722
0.10	205.85	98.225
0.15	90.08	41.978
0.20	61.40	31.659
0.30	43.02	22.635
0.5	32.51	22.038

Table 9. All collapse coefficients.

h/P	C_1	C_2	C_3	C_4	C_5	C_6	C_7
0.05	0.3636	18.096	72.414	1024.78	49.583	131.213	-379.06
0.10	0.3527	16.798	38.587	152.04	26.976	34.669	-53.81
0.15	0.2986	15.483	28.323	67.53	24.811	22.379	-22.55
0.20	0.2846	12.303	28.508	46.53	20.956	21.503	-14.87
0.30	0.3409	6.764	28.653	32.83	15.477	20.158	-10.19
0.50	0.3893	3.272	18.373	25.09	4.229	17.362	-7.47

Figure 6. Collapse Surface for h/P = 0.05

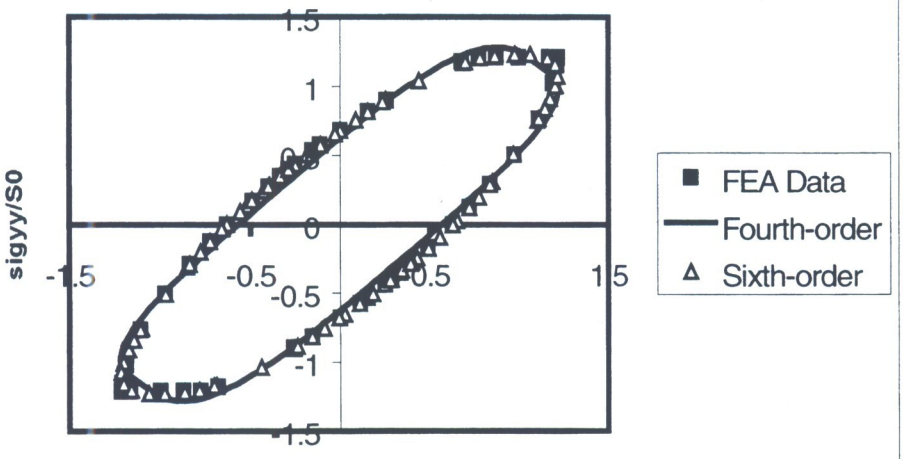

Figure 7. Collapse Surface for h/P = 0.20

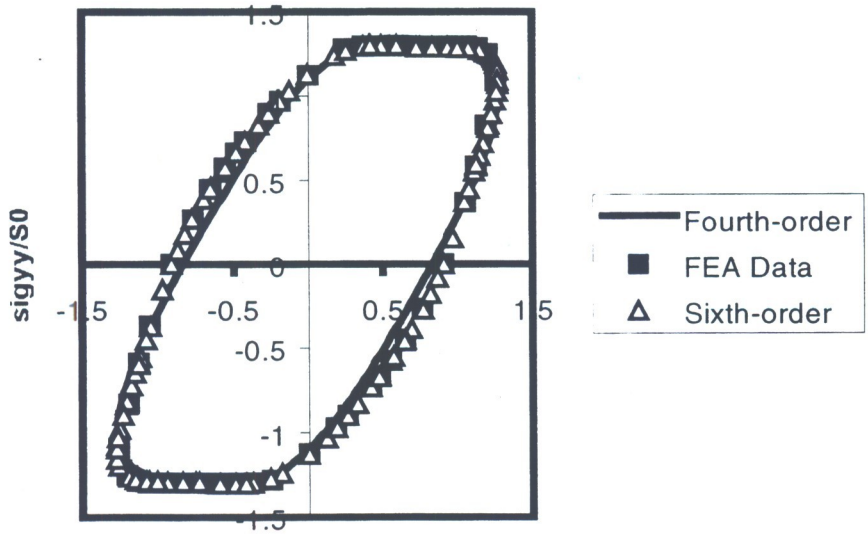

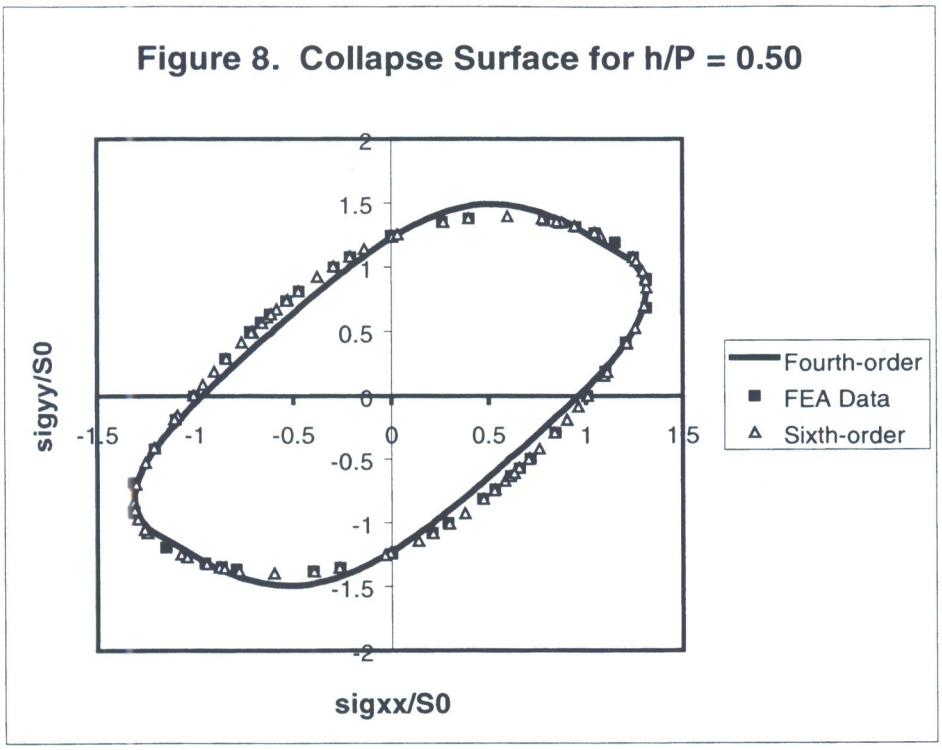

Table 10. Accuracy assessments

h/P	*EQ*	*Number of Points*	*Average Error (%)*	*Maximum Error (%)*
0.05	4^{th}	25	6.63	12.24
	6^{th}	25	0.73	2.33
0.10	4^{th}	18	6.65	11.56
	6^{th}	18	0.96	2.60
0.15	4^{th}	19	6.02	11.43
	6^{th}	19	0.66	2.56
0.20	4^{th}	26	4.28	11.07
	6^{th}	26	0.47	1.63
0.30	4^{th}	19	5.17	11.08
	6^{th}	19	0.27	0.57
0.50	4^{th}	23	4.46	10.01
	6^{th}	23	0.48	1.51